Research Article | Vol. 34, No. 6 / 23 Mar 2026 / Optics Express 10234
Optics EXPRESS

Holographic recording on a curved substrate: investigation of a method to increase the numerical aperture in holographic optical lenses

JORGE LASARTE,[1,2] KEVIN MURPHY,[1,2] IZABELA NAYDENOVA,[1,2] JESÚS ATENCIA,[3] MA VICTORIA COLLADOS,[3] AND SUZANNE MARTIN[1,2,*]

[1]*Centre for Industrial and Engineering Optics, Physical to Life Sciences Research Hub, Technological University Dublin, Ireland*
[2]*School of Physics, Clinical and Optometric Sciences, Faculty of Sciences and Health, Technological University Dublin, Ireland*
[3]*Engineering Research Institute of Aragon (I3A), Faculty of Science, Universidad de Zaragoza, Zaragoza, Spain*
[*]*suzanne.martin@tudublin.ie*

Abstract: This study investigates methods to enhance the numerical aperture (NA) of holographic optical lenses (HOLs) through innovative holographic recording techniques. The research explores the limits of conventional holographic recording of high NA lenses and presents a novel curved-recording technique with the potential to go beyond these limits. The objective is to obtain high NA HOLs suitable for use with LED sources and other highly-diverging input beams. The work first outlines how the maximum numerical aperture lens achievable through holographic recording is limited by the recording geometry. Next, the effect of curving the substrate during holographic recording, and later returning it to a planar shape for use, is explored in order to demonstrate that this could provide a means of fabricating a higher numerical aperture lens. HOLs are then recorded experimentally, firstly using the standard approach for high NA; the overlap of two beams at a plane photosensitive film with as large a beam aperture as possible, and the focal point as close to the (planar) photopolymer as the geometry will allow. Then, a similar arrangement is used, but with curved photopolymer substrates. Diffraction angles and efficiencies of the resulting holographic lenses are compared with the theoretically predicted Bragg diffraction. HOLs with a 20 mm aperture and focal lengths as short as 12 mm are demonstrated.

1. Introduction

Volume phase gratings are particularly suited to the fabrication of highly efficient diffractive optics and, when holographically recorded, can provide the versatility needed to design bespoke lenses and collimating elements tailored to specific lighting applications. Typically, holographic optical elements (HOEs) are fabricated via full-field, low-intensity exposure of suitable photosensitive materials to holographic patterns [1,2] generated by the interference of appropriate beams/wavefronts at a photosensitive film or coating. HOEs are a subset of the general category of diffractive optical elements (DOEs) which encompasses all optical elements that re-direct or re-shape light through diffraction rather than refraction, regardless of how the diffractive structure is fabricated. HOEs and HOLs can be made as low-cost, lightweight, flexible thin polymer films and coatings, which could be well suited for use in LED lighting for building structures, lighting, and display. One of the key challenges, however, is in designing transmission-format diffractive lenses that can function with highly diverging light such as that from LED sources.

#586633 https://doi.org/10.1364/OE.586633
Journal © 2026 Received 4 Dec 2025; revised 12 Feb 2026; accepted 24 Feb 2026; published 13 Mar 2026

Optics EXPRESS

These require particularly large numerical aperture holographic lenses to accommodate the input beam emerging from a highly-diverging source.

Optical components with a large numerical aperture (NA) are essential for numerous other applications also, including advanced microscopy, high-resolution imaging, and optical data storage. They are important when using LEDs in a compact form factor system because of the high NA output cone that LEDs typically produce. High-NA optical systems that push the boundaries of resolution and efficiency are under investigation across a number of research areas [3–5]. Within this field, HOLs have emerged as a promising technology due to their flexibility in beam shaping, compact form factor, and wavelength-specific capabilities [6]. Recent advances in HOE research include applications in wavefront correction, optical trapping, and beam multiplexing, with notable activity in both low and high NA systems [7–9]. For instance, HOEs have been used in augmented reality headsets and compact spectrometers, where they are optimized for specific wavelength ranges and functionalities, albeit often with relatively low NA requirements [10].

Previous work in this area has included various curved holographic elements, but these efforts have primarily focused on high radii of curvature and holograms intended for use while curved [9,11,12] rather than utilizing a curved-to-flat approach.

This paper presents a novel technique using curved substrates during holographic recording to increase the final numerical aperture of a transmission HOL once it is has been returned to a planar shape for use. It investigates, theoretically and experimentally, the increase in NA that curving the substrate during recording can provide, with a view to making them more suitable for use with LEDs. The current work explores the approach by curving in one plane only which is useful for cylindrical lens elements often used with LEDs but could also pave the way for more sophisticated systems. In addition, with modern 3D printing techniques, there is significant potential to holographically record with the photosensitive film supported in asymmetric curves, paraboloids and bespoke 3D surfaces which could be designed to minimize aberrations or produce bespoke diffracted wavefronts, once returned to a planar shape. This paper explores the limitations of existing approaches and leverages innovative recording techniques to increase numerical aperture.

1.1. Holographic recording of high NA lens elements (HOLs) – limiting factors

It has long been understood that the maximum achievable numerical aperture in holographic optical elements (HOEs) is subject to fundamental constraints. These arise from the geometry of holographic recording with overlapping beams, material limitations, and, for elements designed to have a single diffracted beam, the need to maintain high 'volume' or 'Bragg' diffraction across the lens. Each of these factors imposes practical limits that must be considered in both the design and fabrication of HOLs [13,14].

1.1.1. Avoiding 'zero spatial frequency' regions in the grating structure

Holographic recording of a high-NA transmission HOL requires the interference of two beams at the hologram plane, at least one of which should have a non-zero NA (in order for the HOL to have some optical power) with both beams approaching the hologram plane from the same direction. The inter-beam angle, which determines the grating period, therefore varies locally across the HOL's aperture. Early studies of HOL properties pointed out that [13] there is a minimum angle required between the interfering beams to ensure that the spatial frequency is kept above zero at all points on the hologram. Figure 1 shows a typical recording scheme. A diverging beam (shown in blue) and an off-axis collimated beam (shown in green) overlap at a photopolymer layer (PP) resulting in varying local inter-beam angles $\Delta\theta_1, \Delta\theta_2, \Delta\theta_3$, which will each produce different spatial frequency gratings. Since $\Delta\theta_1$ reduces to zero when the central inter-beam angle $\Delta\theta_2$ equals Φ, the spatial frequency will only be greater than zero everywhere

Optics EXPRESS

on the lens if $\Delta\theta_2 > \Phi$ giving the limitation shown in (1). This is important because regions where the interfering beams are co-linear result in extremely low spatial frequency regions in the interference pattern and therefore no diffraction in the HOL. It is important to note that $\Delta\theta$ is considered the interbeam angle and is composed by the angles of the beams B_1 and B_2 used during the recording, and is expressed as $\Delta\theta = \theta_2 - \theta_1$.

$$\Delta\theta > \Phi \tag{1}$$

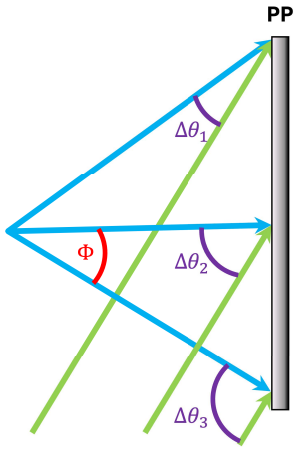

Fig. 1. Typical recording arrangement for a transmission-format HOL, showing how the inter-beam recording angle varies across the element. This example shows the combination of a diverging (blues lines) and a collimated (green lines) beam. Angles $\Delta\theta_1, \Delta\theta_2, \Delta\theta_3$, are the local inter-beam angles that determine the local spatial frequency in the hologram/grating. Φ is the numerical aperture of the diverging beam. PP indicates the photosensitive photopolymer recording medium. Color is for illustration purposes only.

1.1.2. Maintaining a single diffracted order across the HOL (Bragg diffraction / volume regime constraint)

For many applications in lighting and photonics systems, it is desirable for the HOL to produce a single diffracted beam rather than a number of diffracted orders. To ensure this, it is necessary to determine whether operation of the HOE is in the volume holography regime, suppressing higher orders/unwanted beams. Q is useful in determining the threshold for volume behavior especially if the thickness of the material is known, and is defined as:

Q, also known as the Cook-Klein parameter [15], is expressed as:

$$Q = \frac{2\pi\lambda T}{n\Lambda^2} \tag{2}$$

where: λ is the vacuum wavelength of the recording light, T is the thickness of the holographic recording material, n is the average refractive index of the material, Λ is the grating period.

$Q > 10$ [16] is generally accepted as the criterion for ensuring that any higher order beams present are less than one per cent of the total transmitted light.

Q is also convenient, because it depends on the physical thickness of the grating, which is usually known. However, it should be noted that Q has been shown to be less reliable for higher-efficiency gratings. The Rho factor introduced by Moharam and L. Young [17,18] considers Δn independently of the physical thickness and provides a more accurate prediction.

Optics EXPRESS

The grating period Λ, which plays a central role in both equations, is a geometric function of the interbeam angle $\Delta\theta$ and is expressed as:

$$\Lambda = \frac{\lambda}{2\sin(\Delta\theta/2)} \tag{3}$$

This relationship connects the recording geometry used to produce the interference pattern to the spatial frequency in the hologram [19]. It should be noted that the Bragg angle for reconstruction will equal $\Delta\theta/2$ as long as the reconstruction wavelength is the same as the recording wavelength.

Equation (2) combined with Eq. (3) can be used to determine the minimum inter-beam recording angle required to keep Q>10, for a given wavelength λ and material parameters such as T and Δn.

$$\Delta\theta = 2 * \arcsin\left(\frac{\sqrt{5\lambda}}{2\sqrt{\pi T n}}\right) \tag{4}$$

Thinner materials and longer reconstruction wavelengths will require a greater inter-beam angle to ensure Q≥10 and there are no additional diffracted orders. So, in addition to the above requirement described by Eq. (1) we must consider the requirement Eq. (4), with the grating period calculated based on the minimum interbeam angle across the element.

1.1.3. Optics size constraint (Impingement)

Lastly, the physical size of the optical components used in the recording setup will impose a limit on the numerical aperture that can be attained. This limit will also be influenced by the size of the recording area and the distance between the optical elements and the recording plane. The typical recording arrangement for holographic recording of a high NA HOL is shown in Fig. 2.

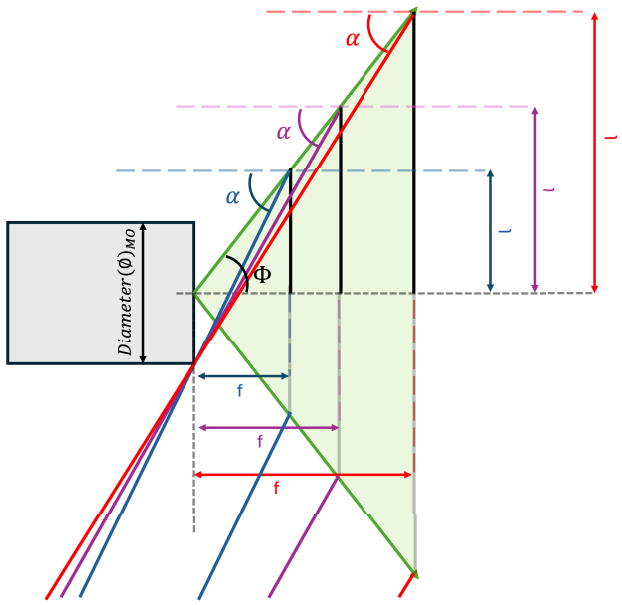

Fig. 2. Schematic representation of the α and Φ angles, showing how the physical width of the optical element constrains beam impingement and influences the resulting angular distribution. Three possible recording planes and off-axis beams are shown, coded by colour, f represents the focal length, and l is half the width of the recorded, for each recording plane.

Optics EXPRESS

The set-up is shown as viewed from above. A high NA beam (shaded in green) is emerging from a microscope objective (MO) and overlapping with a collimated beam that arrives from the bottom left of the diagram. Three potential recording planes are shown (color coded blue, purple and red) together with the corresponding l and f for that plane, and with the second (interfering) beam, appropriate for that recording plane, coded in the same color. For holographic recording to occur at any given point on the recording plane, the two beams must overlap at that point. Any impingement of either beam will prevent recording at that location and lower the NA of the recorded element. This can be one of the most significant challenges when attempting to record high NA HOEs. The placement and size of the lenses and lens housing can introduce the need for a significant off-axis angle in the second interfering beam. Even in systems where Bragg functionality is not important, lower inter-beam angles and on-axis elements require some beam combining element in order to avoid impingement. For high NA recordings of this type it is usually the aperture of the beam combiner which will restrict the NA of the recording beams. In practical systems, the highest NA recording beams can usually be provided by MO lenses. For example, MO as high as NA = 0.9, with a diameter of 29 mm are available from suppliers such as Thorlabs.

The angle Φ can be expressed as

$$\Phi = arcsin(NA) = arctan(l/f) \tag{5}$$

where l is the half of the recording plane width and f is the recording distance (and ultimately the HOE focal length).

The minimum α angle needed to avoid impingement from the diameter of the MO can be determined as:

$$\alpha = arctan(\frac{\frac{\varnothing}{2} + l}{f}) \tag{6}$$

$\varnothing/2$ is half the diameter of the objective lens. This expresses the minimum offset angle needed to be determined as a function of focal length in order to avoid impingement, as long as the diameter and NA of the optic used in recording is known.

As can be seen from Fig. 2, the off-axis angle required to ensure full overlap increases as the distance to the hologram recording plane (the focal length of the HOE) decreases.

1.2. Holographic recording of high NA lens elements (HOLs) using curved substrates

The concept of recording on curved substrate is that by altering the curvature of the recording medium within the overlapping beams, it should be possible to record patterns with fringes that are more slanted than otherwise possible, augmenting the capacity of the HOE to deal with highly diverging beams, once the sample is returned to a planar shape. A theoretical model was developed to explore this, which is outlined below.

Figure 3 shows a schematic of the arrangement for the recording of a HOL via recording on a curved substrate recording (on the left) and for the reconstruction of the flattened HOL (on the right). In this example, during recording, the diverging beam (depicted in green) approaches the recording medium on-axis and (z_0) is the distance from the focal point of the beam to the centre of the photopolymer film, which is supported such that it has a radius of curvature R. The distance l, represents half of the chord of the circumference formed by the ends for the curved recording, and as stated before, will be half of the recorded width for a flat recording, while L represents half of the width of the recorded area once flattened which will be slightly longer (length of the Arc rather than length of the Chord), unless the radius of curvature R is too small, it can be approximated to $L = l$.

The aim of the modeling is to estimate, after flattening the photopolymer, what improvement in numerical aperture can be expected through curved recording, what are the new angles of

Optics EXPRESS

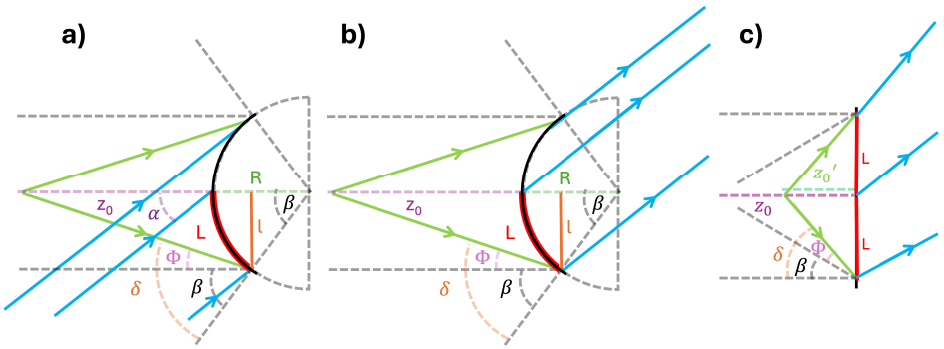

Fig. 3. Schematics of the recording and reconstruction geometries for holographic recording on a curved substrate, with the corresponding mathematical parameters used in the analysis; (a) recording on a curved substrate, (b) reconstruction when the substrate is curved, (c) reconstruction when the substrate is flat.

incidence that will give maximum Bragg diffraction and which new LED-HOE distance will maximize the Bragg match, i.e. the new focal length, z_0'.

From the geometry in Fig. 3, the relationships between β, Φ, δ, expressed in radians, L and z_0' are calculated as follows:

$$\beta = \sin^{-1}\left(\frac{l}{R}\right) \tag{7}$$

$$\Phi = \tan^{-1}\left(\frac{l}{z_0 + R(1 - cos(\beta))}\right) \tag{8}$$

$$\delta = \Phi + \beta \tag{9}$$

$$L = R * \beta \tag{10}$$

$$z_0' = \frac{L}{tan(\delta)} = \frac{R * \beta(rad)}{tan(\delta)} \tag{11}$$

From Fig. 3 it can be extracted that z_0' is smaller than the original z_0, so that during reconstruction the source can be placed at a closer distance, increasing the NA of the system (ultimately better capturing the output of a divergent source like an LED). It is important to note that in practical systems the recording and curvature parameters will have to be carefully chosen so that after flattening the curved recording the rays behave as desired, for example to have to focus into a point with a small error (minimizing spherical aberration) or produce a collimated output. For example, in the reconstruction diagram in Fig. 3, it can be observed that the diffracted beam becomes divergent instead of collimated.

It should also be noted that the value of (z_0') estimated here is accurate only for the holographic grating recorded at the edges of the HOE at distance L from the centre. The exact point at which the rays cross the optical axis varies for different points on the (flattened) HOE. This produces an effect similar to spherical aberration in a refractive lens, where the rays across the optical axis at a range of points along the axis rather than a single focus.

2. Materials and methods

In order to directly compare recording on curved substrate with conventional geometrical methods (recording on a flat substrate), both methods are tested experimentally with a view to exploring their capacity to enhance the operational NA achieved for holographic optical lens elements (HOLs). Two sets of experiments are performed: (1) Recording of HOLs using standard

Optics EXPRESS

holographic recording on a flat surface, while keeping the focal point as close as geometrically possible to the recording plane vs (2) Using a similar optical arrangement while recording with a curved surface geometry to then be reconstructed with a flat geometry. Recording arrangements, photosensitve materials, sample preparation and testing methods are outlined below.

2.1. Photosensitive material

Bayfol HX200 [20] was used for the holographic recording. This is a commercially available material, sensitive to a wide range of wavelengths between 400 and 700 *nm*, that has been used in holographic applications, such as holographic solar combiners [21], with great results and very high diffraction efficiency for some time [22]. Composed of three layers: substrate, photopolymer layer of 16 μm and protective film, it is flexible, but can be laminated onto a rigid substrate in order to give the layer the stability required when recording the holograms.

2.2. Holographic recording – conventional approach

Figure 4 shows the holographic recording arrangement on the left, and a conventional reconstruction arrangement on the right. Two coherent collimated beams from a 532nm laser (Coherent Verdi) are split and recombined at the photosensitive plate in the conventional manner. A microscope objective in one of the beams provides a high Numerical Aperture beam at the recording plane. For maximum NA in the recorded transmission HOL, the microscope objective (MO) of 40x has been brought as close to the photopolymer (PP) as possible without it obscuring part of the other recording beam (z_0 = 25 *mm*) and with an l = 10 *mm*. After splitting, each beam is filtered and expanded with a spatial filter (SF1 and SF2) and collimated (CL1 and CL2). A mirror (M3) allows adjustment of the angle of interference between the two beams. SF 1 is composed of a x20 microscope objective (MO) and a pinhole of 30 µm, whereas SF 2 is composed of a x5 microscope objective (MO) and a pinhole of 20 µm. Pinholes and MOs used for the two beam are not identical because of the off axis nature of one of the beams.

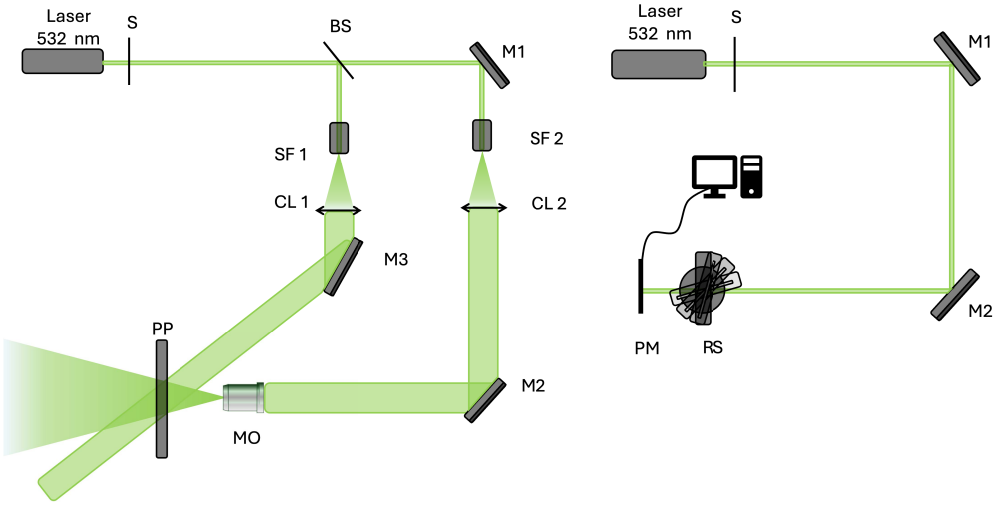

Fig. 4. Holographic setup used for a) recording (left) and b) reconstruction (right).

For the reconstruction arrangement, a rotational stage (RS) and a power meter (PM) are introduced in order to perform a Bragg analysis of the samples. This will be later explained in the testing and analysis section.

Optics EXPRESS

2.3. Holographic recording – recording on a curved surface with planar reconstruction

Recording on a curved surface was carried out for five different HOL types, made with three different recording geometries/arrangements of recording beams and two different radii of curvature. In Table 1 the parameters used for the recording of the samples are shown.

Table 1. Parameters for the recording curved holograms. z_0 being the distance of recording, B_1 *intensity* and B_2 *intensity* being the beam intensities used during the recording.

Geometry	z_0 Distance (mm)	B_1 intensity (mW/cm^2)	B_2 intensity (mW/cm^2)	I_{total} (mW/cm^2)	Contrast	t_{exp} (s)
1	25	0.71	0.74	1.45	0.99	6.9
2	25	0.51	0.84	1.35	0.99	7.4
3	25	0.35	0.75	1.10	0.97	13.6

Using the recording setup shown in Fig. 4 and by changing the inter beam angle as well as the divergence of the object beam (using a microscope objective lens), three different holographic recording geometries were arranged with:

- Geometry 1: B_1 collimated beam at -19° and B_2 collimated beam at 19°
- Geometry 2: B_1 collimated beam on axis at 0° and B_2 collimated beam at 38°.
- Geometry 3: B_1 diverging beam on axis at 0° and B_2 collimated beam at 38°.

38 degrees was the minimum inter-beam angle deemed necessary to avoid impingement in our particular setup. 0 degrees and 38 degrees were therefore chosen as the as the recording angles for the ideal test arrangement, with the on-axis recording beam as the one that is diverging (Geometry 3). This is suitable for a HOE that should function, once flattened, for a LED approaching the HOE along the normal and is the targeted design. This arrangement produces both highly slanted fringes, and contains a wide range of spatial frequencies. In order to better understand any effects of having a large spatial frequency range and slant/shrinkage in the element during curved recording, a simple grating was also studied, having the same off axis 38 degree interbeam angle (Geometry 2) but using two collimated beams for recording. Finally, grating was also recorded with two collimated beams at -19,+19 (Geometry 1) for a comparison with a grating having zero spatial frequency range and zero slant. The only recording geometry that produces a HOL rather than a grating is Geometry 3. Geometry 1 and 2 are simpler geometries used to help quantify the effects of curved recording and to validate the model. The recording medium was curved with two different radii of curvature when used with these three geometries: R=12.5mm and R=30mm, which we will refer to as R1 and R2. The recording setup is similar to that introduced previously in Fig. 4 with the replacement of the flat holder with a curved one that was also custom 3D printed shown in Fig. 5.

2.4. Hologram testing and analysis

The reconstruction setup depicted in Fig. 4 is used to test the recorded HOLs which are mounted on a rotational stage. The testing protocol involves probing the microstructure with a 1.5 mm diameter laser beam while rotating the HOL and monitoring with a power-meter. The power meter is connected to a computer with a software to measure the diffraction efficiency and plot it as a function of angle of incidence. Since only volume elements are being analysed here, only zero order is measured, and from it, the intensity is determined by subtracting the zero order from the total incident radiation. All values are normalized to the intensity of the probe beam

Optics EXPRESS

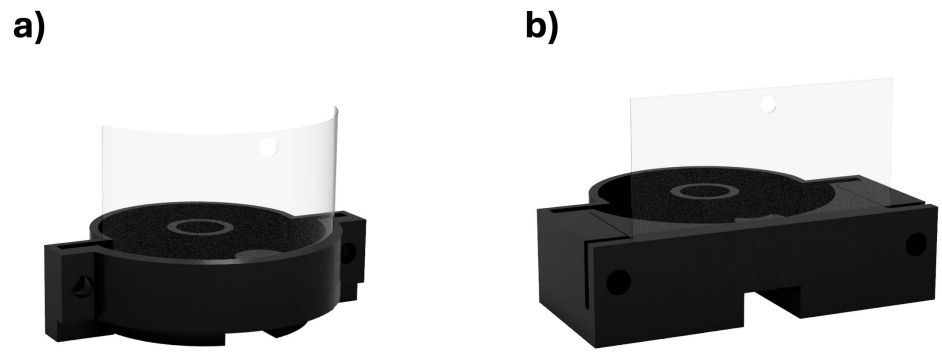

Fig. 5. 3D Printed (a) curved holder for the recording on the left, and (b) flat holder for the reconstruction.

transmitted through unpatterned photopolymer. The obtained data is then used to extract the two angles at which the DE is highest so that it can be compared with the theoretical data. The HOLs were recorded with a total beam intensity (both beams) of $1.4 mW/cm^2$ and all the parameters are seen in Table 2.

Table 2. Parameters for the recording of the regular flat holograms.

z_0	B_1 intensity	B_2 intensity	I_{total}	Contrast	t_{exp}
(mm)	(mW/cm^2)	(mW/cm^2)	(mW/cm^2)		(s)
15	0.51	0.84	1.38	0.99	7.4

2.5. Sample preparation

A flexible transparent polycarbonate plastic of 125 μm thickness is used as a stable substrate on which to laminate the photopolymer Bayfol HX200 [20] for stable holographic recording, while being capable of the necessary deformation for the curved experiments. Plastic supports of approximately 40 x 50 mm with 4 mm laser-cut holes, positioned for optimal clamping and minimal tensions, are placed near the edges of the substrate. A self-adhesive black PVC sheet (Aironfix 370 AF) is adhered to the back of the plastic to remove the undesired back reflections when recording. The photopolymer, 20x40 mm, is then cut to shape and laminated with the photopolymer layer facing the plastic plate.

At first the sample preparation described above was also used for recording on a curved surface. However, as described in the results section, it became necessary to alter the procedure to ensure that the stresses in the active photopolymer layer were minimized. The two alternative arrangements are shown in Fig. 6. Image a) depicts the three layers that constitute photopolymer Bayfol HX200; a protective PE film depicted in yellow ($40\mu m$); the photopolymer itself depicted in green ($16\mu m$) and a TAC substrate depicted in dark blue ($60\mu m$). In image b) the PE film has been removed and the viscous and sticky quality of the photopolymer layer allows to laminate it onto the plastic layer as per its usual use described above. In image c) on Fig. 6 the improved lamination method is shown in which where Thorlabs Optically Clear Double-Sided Adhesive Tape (OCA) (depicted as the red layer) is used to attach the TAC layer to the support, thereby protecting the photopolymer layer from the strains produced by direct adhesion and allowing the TAC layer to absorb the mechanical stress induced by curving the photopolymer.

Optics EXPRESS

z_0	B_1 intensity	B_2 intensity	I_{total}	Contrast	t_{exp}
(mm)	(mW/cm^2)	(mW/cm^2)	(mW/cm^2)		(s)
15	0.51	0.84	1.38	0.99	7.4

Table 2. Parameters for the recording of the regular flat holograms.

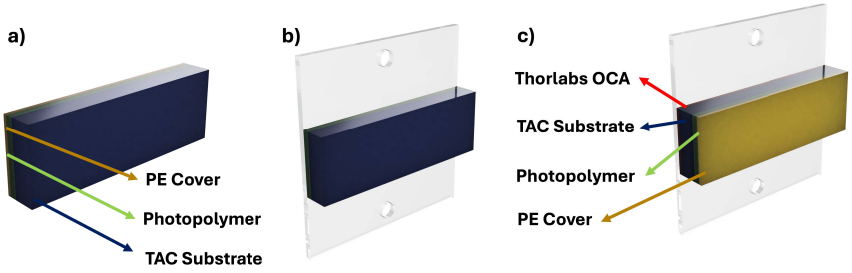

Fig. 6. Bayfol HX material and lamination methods. a) Bayfol HX layers: PE removable cover (yellow), photopolymer (green) and substrate (dark blue). b) the first lamination method, yellow PE cover has been removed for application of photopolymer directly to substrate and c) new lamination method: Bayfol film is reversed, PE is not removed and Thorlabs OCA tape (red) is used to bind the Bayfol to the flexible plastic support.

3. Results

3.1. Theoretical modeling of the change in beam angles

Using the theory outlined above (Eqs. (7)–(11) and Fig. 3) A model was developed to calculate the changes in diffraction behavior expected when a HOL that has been recorded on a curve in a flexible medium is later returned to a planar shape. The expected change in grating Bragg angles due to the change in curvature and consequent change in the optimum incident and diffracted rays for the element were calculated. The model assumes that the structure and substructure of Bragg planes deforms with the substrate and conforms to its new shape.

Figure 7 shows the rays representing the beams for the three recording geometries, recorded on a substrate with a radius of curvature 30 mm (R2). The top row shows the different recording beams during recording, meeting at the curved photopolymer layer. Since recording and reconstruction wavelengths are identical, these would also be the rays and angles that give maximum Bragg diffraction for reconstruction, and the middle row shows the appropriate rays for Bragg-matched reconstruction in the still-curved photopolymer. The lower row shows the new beam directions needed for maximum Bragg diffraction after the curve has been flattened into a planar shape. Colour is for illustration purposes only, all light rays are of the same wavelength. It can be clearly observed from Fig. 7 that the directions of all beams are changed. For example, for Geometry 3 the focal point is moved much closer to the photopolymer, achieving the desired effect of increased NA, and confirming the potential for using curved recording as a means to producing higher NA HOEs.

However, it should also be noted that the divergence of the originally-collimated recording beams is also altered, and this would need to be taken into account when designing devices that require specific input and output beams. In addition, although it is not particularly noticeable in this figure, it should be borne in mind that the rays in the flattened HOEs do not converge to a perfect focal point and some spherical aberration is therefore also introduced. For example,

Optics EXPRESS

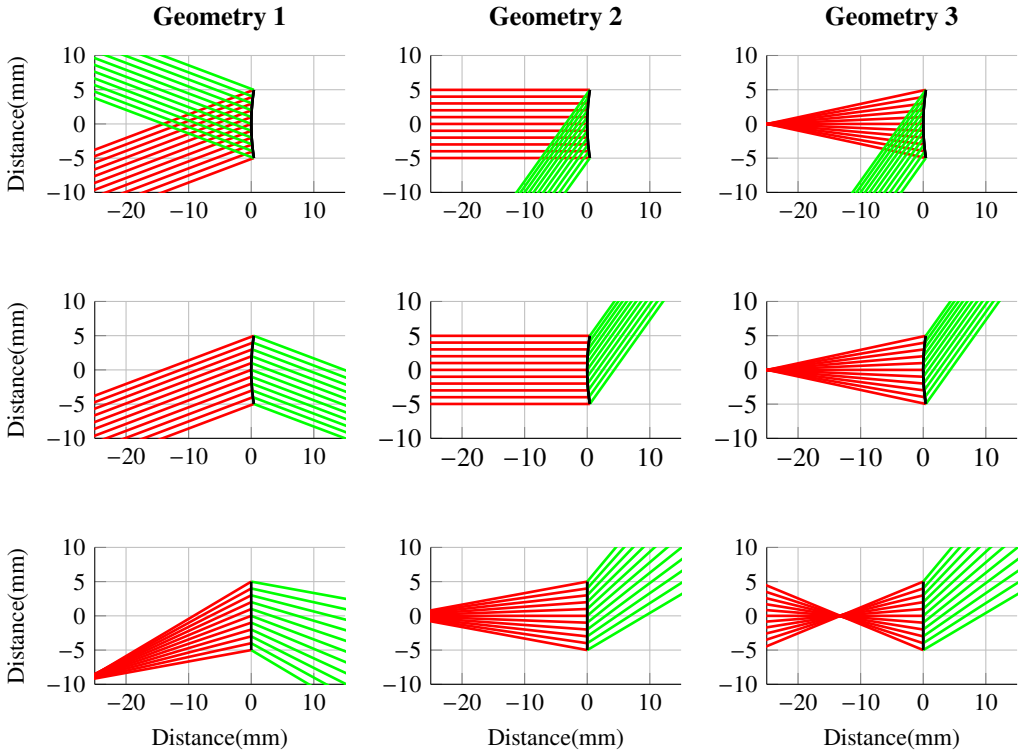

Fig. 7. Diagrams depicting the rays for recording and reconstruction for the three different recording geometries, illustrating the change in ray paths when the photopolymer is flattened. Top row shows recording geometries on the curved substrate; middle row shows reconstruction while the substrate is still curved; bottom row shows the corresponding reconstruction geometries once the substrate has been flattened. Here, curvature radius $R2 = 30mm$ for top and middle row, and $R = \infty$ returned to the planar shape for reconstruction.

in Fig. 7, Geometry 3 spherical aberration can be estimated as 1.5 mm along the optical axis. This would be considered acceptable since from previous work [23] it was observed that a focal point error of 2 mm would be acceptable for efficient performance of a similar HOE, but this is nevertheless an additional limitation, especially for short radii of curvature and large apertures.

3.2. *Modelling the factors that limit numerical aperture of HOLs*

As discussed in Section 1.1, there are three key factors that limit the numerical aperture of holographically recorded lenses (HOLs). Each imposes a minimum offset/inter-beam angle that needs to be introduced in the recording setup to avoid the particular issue: zero spatial frequency zones, higher order beams or partial recording of the beam diverging due to impingement. Figure 8 plots these limits expressed in terms of the minimum recording offset angle as a function of the HOE focal length.

In the case of limiting factor 1, the need to avoid parallel recording beams and zero spatial frequency zones, we assume that the diverging recording beam is produced by a microscope objective NA of 0.9 initially and then 0.6 for comparison. The absolute minimum inter-beam angle needed to avoid this limit is simply calculated from Eq. (5). Limiting factor 1 exists for every HOL even if there is no requirement that they function in the volume regime.

Optics EXPRESS

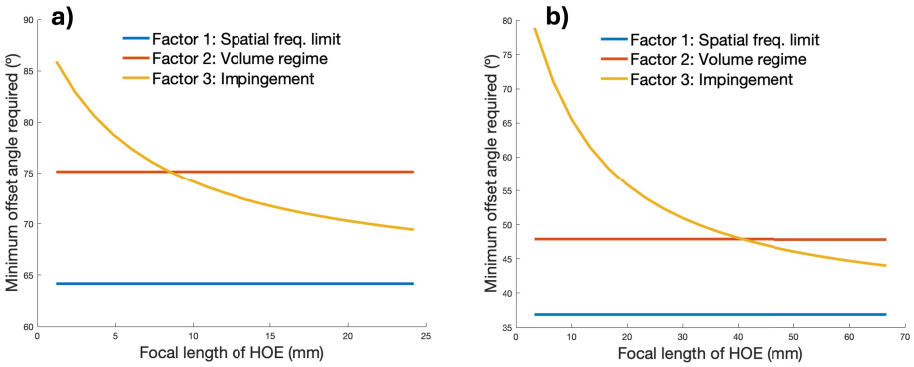

Fig. 8. The calculated minimum offset angle required as a function of the focal length of the HOE lens, with fixed HOE lens numerical aperture,(a), NA= 0.9 and (b), NA= 0.6. The yellow line represents the limit from the geometrical constraint. The red line depicts the angles for which recording within volume regime. The blue line represents the minimum recording angles for the minimum spatial frequency.

For limiting factor 2, the need to avoid multiple additional order beams, the minimum inter-beam angle that ensures Q>10 is calculated using Eq. (4): letting $n = 1.5$, $\lambda = 532nm$ and assuming thickness of photopolymer layer $T = 14\mu m$.

Finally, in order to calculate the minimum angle needed to avoid impingement, for limiting factor 3, the MO diameter is set to $\varnothing = 29mm$, then using Eq. (6) a minimum angle for each focal length is calculated, l increases accordingly to maintain the desired NA.

In Fig. 8 the three separate limits are shown. At shorter focal lengths, the limit for impingment becomes increasingly restrictive and the other two limits, although they impose significant restrictions, do not vary with focal length. It is demonstrated that a reduction in the focal length requires an increase in the minimum offset angle for a fixed recording aperture. Consequently, achieving shorter focal lengths requires a trade-off between the desired focal distance and the size of the effective recording area.

Figure 8 also demonstrates that reducing the numerical aperture of the recording beam reduces all three restrictions very significantly, however this of course also limits the NA of the HOL that can be recorded. The next step was therefore to investigate whether it could be possible to work with lower NA recording beams add additional optical power through recording on a curved substrate.

Figure 9 (a) shows the ratio of the reconstructed focal length z_o' to the recording focal length (the distance from the recording beam focus to the recording plane) z_o to investigate the improvement possible with curved recording. The dependence of the resulting numerical aperture in the recorded HOL (once flattened) on the curvature used during recording is shown in b). For both graphs, the dependence is plotted for a number of z_o values, typical during holographic recording of high NA elements.

The first observation from the graph is that z_o/z_o' is highest, indicating the greatest improvement, at short radii of curvature and tends towards unity at longer radius. This confirms that a curved recording provides a shorter effective focal length compared to a flat recording. Data for radii of curvature shorter than L (half the length of the recording area) were not plotted due to the impracticality of such curves in a real recording arrangements. When the numerical aperture (NA) is plotted, the results show a systematic increase in NA as the radius of curvature is reduced. Although the HOEs recorded with longer focal lengths show the largest relative improvement in their focal length, the highest NA is achieved for small design focal lengths (E.g.:z_o = 15–30

Optics EXPRESS

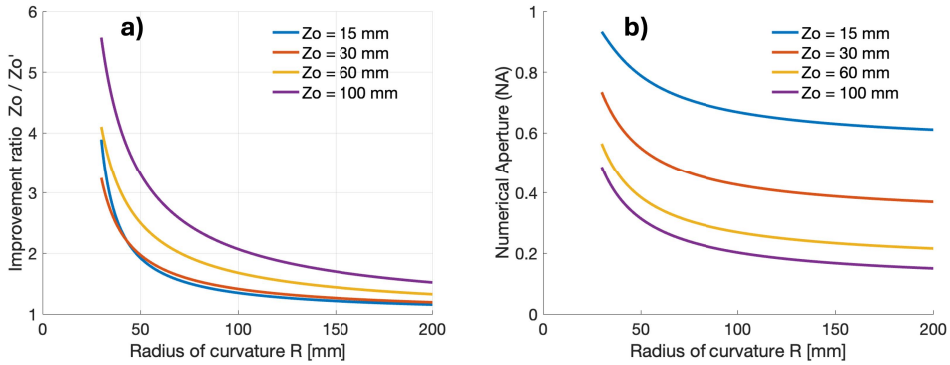

Fig. 9. Graphs showing (a) the evolution of the z_0/z_0' ratio and (b) the numerical aperture as a function of the radius of curvature for a series of z_0 values . Here, z_0 denotes the recording distance, while z_0' represents the reconstruction distance after flattening the holographic element. L is fixed at 20 *mm*.

mm). These results confirm that employing a curved recording geometry could significantly improve the numerical aperture of the diffractive element.

3.3. Experimental tests using conventional holographic recording

As a first step toward experimental validation, standard holographic recording methods were used to record HOLs with the highest numerical aperture that could be achieved by the conventional method, given the practical constraints already mentioned. The procedure is detailed in Section 2.2 using Geometry 3. In order to test the recorded HOL and to ascertain whether the Bragg diffraction behavior matched that expected, the HOLs were characterized at multiple points across the lens aperture using the Bragg diffraction testing setup illustrated in Fig. 4. These measurements were performed at locations from −5 *mm* to +5 *mm* across the horizontal diameter of the lens in 1 *mm* increments. Both the recording and probing wavelengths were 532 *nm*.

At each probing position, two minima were observed in the transmitted beam, corresponding to Bragg diffraction maxima in the first order of diffraction. These features provide spatially resolved information about the microstructure of the HOL. As expected, one diffraction peak, was observed at the same angle across all measurement points (corresponding to the collimated recording beam), while the second peak shifted relative to the sampling location (as expected for a diverging recording beam/lens with optical power). Although this angular shift was not perfectly symmetrical, it closely matched the behavior predicted by the theoretical model, shown by the blue line in Fig. 10, obtained with the method described in Section 1.2.

The key observation is the close agreement between the measured peak positions and theoretical predictions.

3.4. Experimental tests with holographic recording on a curved substrate

The results of this approach are divided into two subparts: (1) Results for curved recording without modified lamination and (2) Results for curved recording with special lamination.

3.4.1. Results for curved recording without special lamination

In this section of the results, the calculated theoretical Bragg peaks θ_1 and θ_2 introduced in 1.1.1, are compared vs those same ones but measured in different points across the recorded samples experimentally. Figure 11 presents experimental and theoretical data for the angular position of the Bragg peak as a function of the position of the probe beam for an initial set of HOLs recorded using a radius of curvature of 12.5 *mm* for Geometry 1, 2 and 3. The solid lines indicate the

Optics EXPRESS

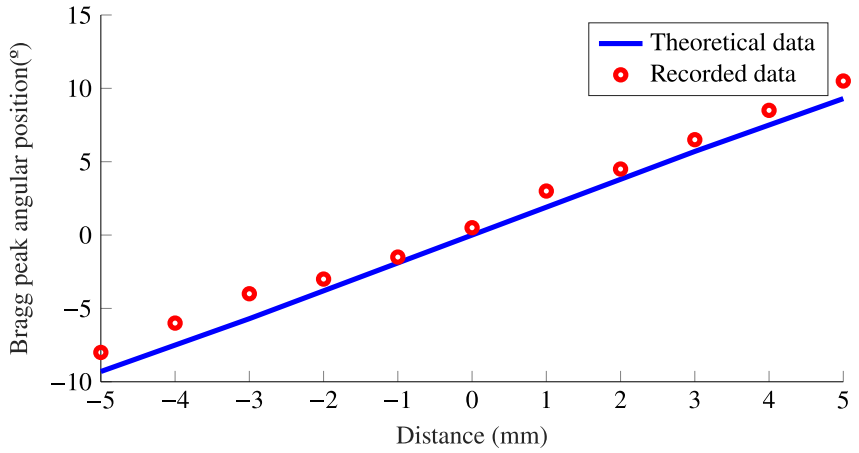

Fig. 10. Results for HOLs recorded with Geometry 3, using conventional holographic recording with 25 mm focal length. The angular position of the Bragg peak as a function of the position of the probe beam location on the HOL is shown. Experimental data (red) is compared with theoretical prediction (blue line).

expected positions of the Bragg diffraction maxima based on the theoretical approach illustrated in 7. The green and red curves represent the "left" and "right" respectively Bragg diffraction maxima in the Bragg curve data shown in the Supplement 1 (they correspond to the minima in that data). Diffraction is most efficient when the incident beam makes and angle equal to the Bragg angle on either side of fringe planes. This means that generally (assuming the fringe slant is not too high) two separate Bragg maxima will be observed if the grating is probed at a wide-enough range of angles. The green curves and points correspond to one set of Bragg peaks and the red indicate the expected angle for the other set.

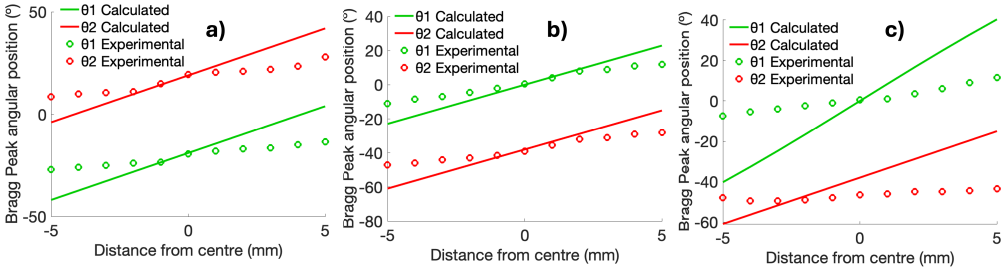

Fig. 11. Results for HOLs recorded on a curved substrate using the first lamination technique. Comparison of the theoretical data obtained by the model (shown as solid lines) vs the experimental data measured at different locations on each HOL. From left to right, HOLs were recorded with Geometry (a) Geometry 1 (+19°,-19°, both collimated), (b) Geometry 2 (0°, 38°, both collimated) and (c) Geometry 3 (0°, 38°, one diverging) all at R = 12.5 mm . From Supplement 1 Figure S1.

These initial experimental results deviated significantly from theoretical predictions, for all three geometries. A poor match with theory is observed, with deviations increasing almost linearly away from the center of the HOL in each example.

Modifications were then made to the radius of curvature. Figure 12 presents the angular position of the Bragg peak as a function of the position of the probe beam for HOLs recorded using a radius of curvature of 30 *mm* and 12.5 *mm*. For simplicity Geometry 1 is used in both. It

Optics EXPRESS

was observed that the longer radius /lower curvature reduced the discrepancy between measured and theoretical values, although the results still fell short of the expected performance.

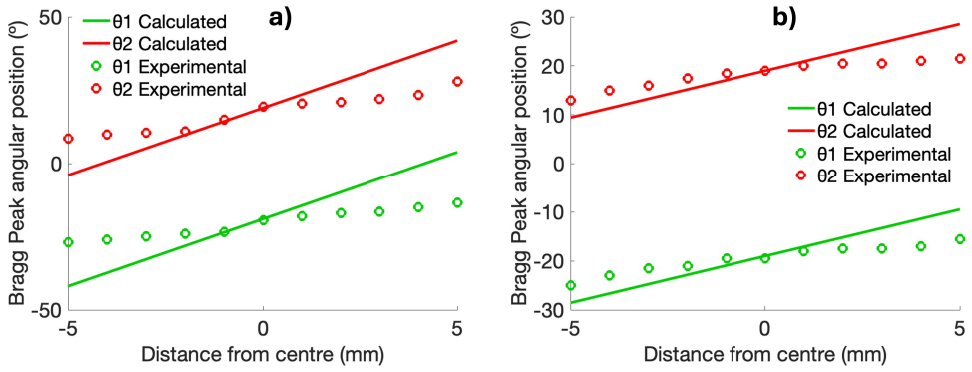

Fig. 12. Results for HOLs using approach 2 - curved recording with the first lamination technique. Comparison of the theoretical data obtained by the model (solid lines) vs the experimental data measured is shown for each HOL. Where Geometry 1 (+19,-19, both collimated) was used to record both and for (a) R = 12.5 mm and (b) R = 30 mm. See Supplement 1 Figure S1 for the individual Bragg Curves.

The improvements observed at a longer radius of curvature point towards stresses in the photopolymer as the most likely cause of Bragg peak deviation. Improved lamination technique aimed at reducing the material stress during the curving and flattening process were therefore investigated.

3.4.2. Results for curved recording with adapted lamination technique

The new protocol for the sample preparation shown in Section 2.5 was then adopted. The longer radius of 30 mm was also retained since it had shown a significantly better fit to the theoretical data. Figure 13 shows similar data for two HOLs recorded using a radius of curvature of 30 *mm* and recording geometries 1 and 3 respectively. Initial recordings were carried out using Geometry 1 for simplicity and after observing some improvement, Geometry 3 which is the preferred geometry. Agreement with theory is significantly improved on the previous results. Geometry 3 is observed to be the best fit with theory. Hence it can be hypothesised that the new lamination technique not only doesn't have any detrimental effects but that it sufficiently reduces the stresses generated by the curving.

Although this study focuses on changes in ray directions and measurement of the change in Bragg angle for the structure recorded, it is worth noting that recording on a curved substrate appears to have no negative effect on diffraction efficiency relative to the standard method, for the examples tested, as long as the improved lamination procedure is used. This can be observed in the Supplement 1 Figure S1.

Figure 14 shows diffraction efficiency data, obtained from the peaks diffraction efficiency of the bragg curves for holograms recorded with the lamination technique utilising Thorlabs OCA tape, in this case using Geometries 1 and 3 with curvature R2. In order to examine the variation across the HOL and compare efficiency data for these three geometries, the Diffraction Efficiency data was normalized to an initial reference point, then plotted at each measurement location.

Table 3 shows the maximum achieved NA experimentally with these HOLs for both methods given that the maximum recorded area is 20 mm for both methodsand reconstructed the focal distances (while in a planar shape) are measured as 25 mm for the conventional recording and 12 mm for the curved recording (+/- 0.5mm). Since for the HOL of the curved recording, the

Optics EXPRESS

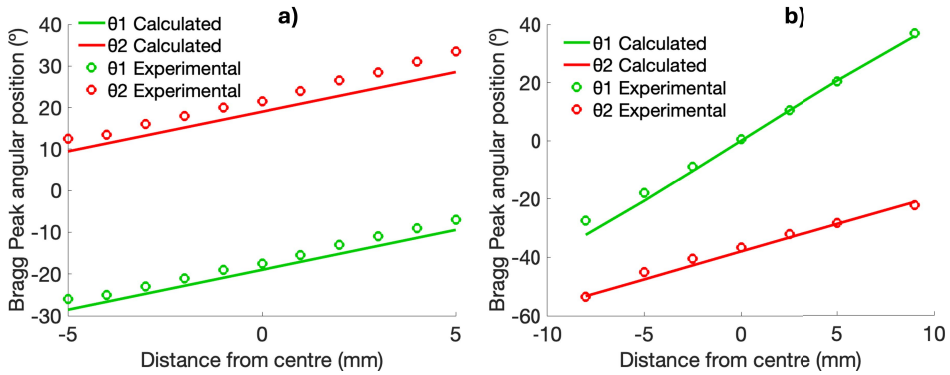

Fig. 13. Results for elements recorded via the second lamination technique at R=30 mm, with (a) Geometry 1 (+19,-19, both collimated) and (b) Geometry 3 (0°, 38°, one diverging). From Supplement 1 Figure S1.

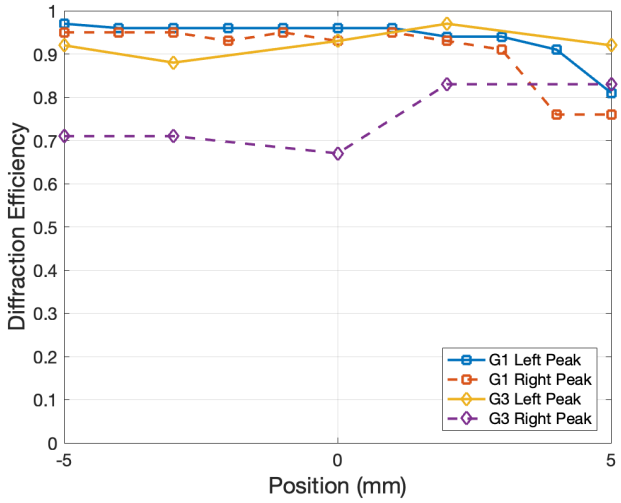

Fig. 14. Diffraction efficiency measured at various points across the hologram. HOLs made with Geometry 1 (+19,-19, both collimated) and 3 (0°, 38°, one diverging) with Curvature R2.

Bragg curves were only measured up to 9 mm to the left and 8 mm to the right, for the calculation of the NA, the considered half width will be $l = 8.5$, hence obtaining 0.58 NA.

Table 3. Comparison of the maximum NA and DE achieved for both methods.

Method	Max NA Achieved	Max DE Achieved	Max NA Theoretical
Standard method	0.37	0.9	0.9
Curved substrate	0.58	0.9	0.9

4. Discussion

The results presented above show that holographic recording on a curved substrate can improve the numerical aperture of the recorded HOL. In the same experimental arrangement that yielded a maximum NA of 0.37 for conventional holographic recording, the curved recording method

Optics EXPRESS

achieved a substantially higher NA of 0.58. To the best of our knowledge, this is the highest NA achieved in a holographically recorded optical element.

It is shown theoretically that significant changes in the incident and diffraction angles occur when a HOL that has been recorded on a curve in a flexible medium is then returned to a planar shape for use. The model provides precise angles at which the new Bragg peak is expected to be observed based on the deformation and also shows that curving introduces aberrations in the output beam. Limitations affecting high NA HOLS are presented (Fig. 8) and it is observed that at short focal lengths and high NA values, the requirement for high off-axis angles to avoid impingement becomes dominant.

The improvement that can be expected from recording on a curved substrate is then presented for a range of curvatures (Fig. 9) as a ratio of initial (curved) NA to final (flattened) NA, which is also the ratio of the focal lengths. It was observed that the biggest relative improvement is for HOLs for which the initial focal length is longer (60 *mm* and 100 *mm*) but the highest NA can be achieved for the HOLs for which the initial focal length is shorter (30 *mm* and 15 *mm*).

It can be concluded that significant additional optical power can be introduced through this approach even for low numerical aperture recording arrangements, and for shorter focal lengths it can help achieve higher NA than are possible in standard systems. Finally the approach has been validated experimentally (Fig. 13). The experimental data for a simple grating (Geometry 1) and an off axis holographic lens with a focal length of 25 *mm* (Geometry 3) was found to agree closely with the predicted values and it was also demonstrated that high diffraction efficiencies ($> 80\%$) are achievable with this approach.

5. Conclusions

Holographic recording on a curved substrate has been investigated with a view to making higher powered HOE lenses than were previously possible. This type of HOE lens, which can be used to re-direct and/or collimate a highly diverging beam, is suited to compact optical systems using sources such as LEDs. Firstly the concept was explored by modelling the effect of recording holograms on a curved substrate, then returning them to a planar shape for use. This was done by calculating the expected change in grating Bragg angles and consequent changes in the optimum incident and diffracted rays. Next, the improvement in numerical aperture that this would confer was modelled for a range of radii ($30 - 200$ *mm*) of curvature and HOL focal lengths. Then, in order to experimentally validate the approach, a number of short focal length HOLs were recorded in Bayfol HX200 while supported in a curved shape, then flattened for testing. The angle of incidence for optimum Bragg diffraction was then measured across the HOL. Initially material stresses led to unexpected results, but with an improved lamination method, a very good agreement (within 2°) was obtained between the calculated Bragg peak position and the experimentally measured ones. Experimentally, 20 mm aperture HOLs were recorded with focal lengths as short as 12 *mm*. In the same experimental arrangement that yielded a maximum NA of 0.37 for conventional holographic recording, the curved recording method achieved a substantially higher NA of 0.58, demonstrating the potential of recording on a curved substrate. However, the approach is not without limitations: Producing a clean, non-aberrated output beam will require careful design of the curved supports used during holographic recording and shadowing can occur for short radii of curvature which limits the NA. In addition, it should be borne in mind that these lenses are cylindrical lenses and the method has been explored here for curvature in only one axis. To the best of the authors' knowledge, use of curved holographic recording as a means to improving the numerical aperture of the recorded HOLs has not previously been studied and the work presented provides the basis for further work in which specific input and output beams can be designed through a combination of radii of curvature and recording beam divergence.

Funding. Taighde Éireann - Research Ireland (20/FFP-P/8851); Diputación General de Aragón-Fondo Social Europeo (TOL research group, E44-23R).

Optics EXPRESS

Acknowledgment. This publication has emanated from research conducted with the financial support of Taighde Éireann (Research Ireland) under Grant number 20/FFP-P/8851, and by the Diputación General de Aragón-Fondo Social Europeo (TOL research group, E44-23R). The authors thank the Physical to Life Sciences Research Hub in TU Dublin, for the technical facilities and administrative support provided as well as the wider team of colleagues in the IEO Centre. Open access funding provided by Irish Research eLibrary.

Disclosures. The authors declare no conflicts of interest.

Data availability. Data will be available at Code Ocean repository at [24].

Supplemental document. See Supplement 1 for supporting content.

References

1. D. Vather, I. Naydenova, D. Cody, *et al.*, "Serialized holography for brand protection and authentication," Appl. Opt. **57**(22), E131–E137 (2018).
2. H. Berneth, F. K. Bruder, T. Fäcke, *et al.*, "Holographic recording aspects of high-resolution Bayfol-HX photopolymer," in *Proc. SPIE*, 7957 (SPIE, 2011), pp. 122–136.
3. S. D. Mellin and G. P. Nordin, "Limits of scalar diffraction theory and an iterative angular spectrum algorithm for finite aperture diffractive optical element design," Opt. Express **8**(13), 705–722 (2001).
4. Y. Zhou, Y. Liu, H. Liang, *et al.*, "Efficient inverse design of large-scale, ultrahigh-numerical-aperture metalens," *Photonics*, **11**, p. 940 2024).
5. Y. Zhou, C. Mao, E. Gershnabel, *et al.*, "Large-area, high-numerical-aperture, freeform metasurfaces," Laser Photonics Rev. **18**(6), 2300988 (2024).
6. C.-W. Ooi, Y. Hiroi, and Y. Itoh, "A compact photochromic occlusion capable see-through display with holographic lenses," *Proc. IEEE Virtual Reality and 3D User Interfaces* , (2023), pp. 237–242.
7. S. J. Byrnes, A. Lenef, F. Aieta, *et al.*, "Designing large, high-efficiency, high-numerical-aperture, transmissive meta-lenses for visible light," Opt. Express **24**(5), 5110–5124 (2016).
8. T. Wang, W. Yu, C. Li, *et al.*, "Biomimetic compound eye with a high numerical aperture and anti-reflective nanostructures on curved surfaces," Opt. Lett. **37**(12), 2397–2399 (2012).
9. W. Wang, G. Chen, Y. Weng, *et al.*, "Large-scale microlens arrays on flexible substrate with improved numerical aperture for curved integral imaging 3D display," Sci. Rep. **10**(1), 11741 (2020).
10. B. C. Kress and M. Pace, "Holographic optics in planar optical systems for next generation small form factor mixed reality headsets," Light: Advanced Manufacturing **3**, 771–801 (2022).
11. P.-A. Blanche and C. T. Draper, "Curved holographic waveguide combiner for HUD and AR display," in *Digital Holography and Three-Dimensional Imaging*, (Optica Publishing Group, 2021), pp. DF2F–4.
12. C. T. Draper and P.-A. Blanche, "Holographic curved waveguide combiner for HUD/AR with 1-D pupil expansion," Opt. Express **30**(2), 2503–2516 (2022).
13. D. Close, "Holographic optical elements," Opt. Eng. **14**(5), 408–419 (1975).
14. J. N. Latta, "Computer-based analysis of hologram imagery and aberrations. i. hologram types and their nonchromatic aberrations," Appl. Opt. **10**(3), 599–608 (1971).
15. W. Klein and B. D. Cook, "Unified approach to ultrasonic light diffraction," IEEE Trans. Sonics Ultrason. **14**(3), 123–134 (2005).
16. H. Kogelnik, "Coupled wave theory for thick hologram gratings," Bell Syst. Tech. J. **48**(9), 2909–2947 (1969).
17. M. G. Moharam and L. Young, "Criterion for Bragg and Raman-Nath diffraction regimes," Appl. Opt. **17**(11), 1757–1759 (1978).
18. T. K. Gaylord and M. Moharam, "Thin and thick gratings: terminology clarification," Appl. Opt. **20**(19), 3271–3273 (1981).
19. V. Toal, *Introduction to Holography* (CRC Press, 2022).
20. Covestro. AG, "Bayfol HX200 description and application information," (2018). https://solutions.covestro.com/en/products/bayfol/bayfol-hx200_86194384-20033146 [Accessed 13-February-2024].
21. M. V. Collados, D. Chemisana, and J. Atencia, "Holographic solar energy systems: The role of optical elements," Renewable and Sustainable Energy Reviews **59**, 130–140 (2016).
22. J. Marín-Sáez, J. Atencia, D. Chemisana, *et al.*, "Characterization of volume holographic optical elements recorded in Bayfol HX photopolymer for solar photovoltaic applications," Opt. Express **24**(6), A720–A730 (2016).
23. J. Lasarte, K. Murphy, I. Naydenova, *et al.*, "Modelling HOE performance with an extended source: experimental investigation using misaligned point sources," in *Proc. SPIE*, 12574 (2023), pp. 16–30.
24. J. L. Sanz, "Raw data for holographic recording on a curved substrate: investigation of a method to increase numerical aperture in holographic optical lenses," 1.0 Code Ocean, (2023), https://codeocean.com/capsule/5648320/tree